IEEE TRANSACTIONS ON CONTROL SYSTEMS TECHNOLOGY, Vol 11, No 5, 2003, pp.612-628 ·

Feedback Controller Design for a Spatially-Distributed System: The Paper Machine Problem

G.E. Stewart, *Member, IEEE*, D.M. Gorinevsky, *Senior Member, IEEE*, and G.A. Dumont, *Fellow, IEEE*

***Abstract*— This article reports on the development and implementation of an algorithm for the design of spatially-distributed feedback controllers for the wide variety of physical processes that are included in cross-directional control of industrial paper machines. The spatial and temporal structure of this class of process models is exploited in the use of the two-dimensional frequency domain for analysis and two-dimensional loop shaping design of feedback controllers. This algorithm forms the basis of a software tool that has recently been implemented in a commercial product and its use is illustrated for tuning CD controllers on two different industrial paper machines. The first example describes the use of the tool in stabilizing an unstable closed-loop system by retuning the distributed controller. The second paper machine example exposes an underperforming controller. Subsequent retuning of the controller resulted in a dramatic performance improvement.**

***Index Terms*— Distributed control, Industrial control, Multidimensional systems, Controller tuning, Frequency domain synthesis, Distributed parameter systems.**

I. Introduction

THIS paper reports on results in the development of algorithms and their implementation in a software tool for the design of a feedback controller of an industrial spatially-distributed system. The papermaking process employs large arrays of actuators spread across a continuously moving web to control the cross-directional (CD) profiles of the paper properties as measured by a scanning gauge downstream from the actuators. A CD control system calculates actuator moves to maintain the measured CD profiles of paper properties on target. Papermaking is an important multi-billion dollar industry – in North America and worldwide – and CD control on paper machines is arguably the most established industrial application of spatially-distributed control.

CD control has been long recognized as an interesting and challenging problem by the control systems community and there have been many papers published studying design of various CD control algorithms. The CD control approaches studied in the literature include robust control design [1], [2], [3], [4], [5], various subspace and dimensionality reduction methods [6], [7], [8], minimum variance control [9], [8], as well as two-dimensional control methods [10]. However, most of the control laws proposed and studied in the above mentioned papers, have not been used in industry, except for some short-term trials.

Online optimization methods such as model predictive control (MPC) are an attractive possibility due to their ability to address hard physical constraints on the actuators. The limitation of these techniques has traditionally been due to the enormous online computational load and their sensitivity to model uncertainty. However advances in computing power coupled with theoretical work in model reduction and robustness (for example [5], [11]) are beginning to make such techniques tractable. Industrial examples of optimization based CD controllers may be found in [12], [9], [13].

Industrial CD control systems have been installed in the field for more than two decades and their algorithms evolved over time to attain an acceptable tradeoff between the achievable closed-loop performance (which requires sophisticated algorithms) and the ease of support and maintenance (which requires simple, easily understandable algorithms for tuning). In the paper industry, simplicity of use is especially important because support and maintenance are typically performed by technician-level personnel. In addition, acceptance of new algorithms (even if they are simple) is usually slow, because there is a large existing base of installed CD control systems. These are typically maintained and supported by their respective vendors. In many CD control installations significant performance improvements can be achieved for an existing controller by implementing a better tuning of the control loop. The tuning problem is to select optimal values for the free parameters within the fixed control algorithms, and CD controller tuning is the main topic of this paper. There is little literature on this topic, the majority of which consists of conference papers by the authors of the present paper [14], [15]. This paper is meant as a first archival publication covering this gap.

CD control tuning has to take into account the usual issues of stability, robustness, and disturbance rejection performance. In addition to that, there are issues of spatial stability and performance of the control that are specific for the CD process control. Closed-loop spatial instability of CD control might be caused by poor controllability of the process at high spatial frequencies. The spatial instability manifested as a picket fence pattern of the actuator setpoints (actuator picketing) is a well known and often encountered problem in industrial CD control installations and indicates a controller that has been designed such that it is chasing uncontrollable components of the error

Department of Electrical and Computer Engineering, University of British Columbia, 2356 Main Mall, Vancouver, B.C., Canada V6T 1Z4. greg.stewart@honeywell.com

Honeywell Industry Solutions, 500 Brooksbank Avenue, North Vancouver, B.C., Canada V7J 3S4.

Honeywell Laboratories, One Results Way, Cupertino, CA, USA 95014.

signal [16].

This paper presents the architecture of a typical industrial CD control system. The tuning algorithms are herein developed for such an architecture. Interestingly enough, CD control systems independently developed by different vendors have many similarities in the structure of the control law, despite the claimed use of various proprietary algorithms for signal processing and control. This is because many existing CD control systems have evolved over time starting from the simplest algorithms and adding controller enhancement as the performance problems with some of the deployed controllers became apparent. The simplest algorithm for CD control is *mapped* or zone-by-zone control where the measured high-resolution profile error is mapped to yield errors for each actuators. The simple mapped CD control does not work well where the CD response of neighboring actuators overlap significantly. This was recognized by the industry and overcome by introducing *error decoupling* and *actuator profile smoothing* terms in the control law. Such an industrial controller structure is considered in this paper.

The design, implementation, and field testing of the CD control tuner described herein was enabled by a use of the automated identification tool described in [17], [18], [19], [20]. The identification provides a CD process model required for the control analysis and tuning. In what follows, the structure of the accepted CD process model and the industrial CD control law structure are discussed in more detail.

Overall, the main contributions of this paper include the following: (i) a thorough study of an industrial CD control engineering problem; (ii) an application of a novel two-dimensional loop shaping design procedure to CD controller tuning; (iii) construction of an industrial software tool for the analysis and tuning of the feedback controller; (iv) presentation of typical industrial results.

A. Notation

This article makes extensive use of banded, symmetric matrices – Toeplitz and circulant. A band-diagonal symmetric Toeplitz matrix of size $n \times n$ with $q < n/2$ degrees of freedom $\bar{a} = [a_1, \ldots, a_q]^T$ will be denoted by,

$$A = \mathcal{T}(\bar{a}, n) := \underbrace{\begin{bmatrix} a_1 & a_2 & \cdots & a_q & 0 & \cdots & \cdots & \cdots & \cdots & 0 \\ a_2 & a_1 & a_2 & \cdots & a_q & 0 & \ddots & \ddots & \ddots & \vdots \\ \vdots & a_2 & a_1 & a_2 & \vdots & a_q & \ddots & \ddots & \ddots & \vdots \\ a_q & \cdots & a_2 & a_1 & a_2 & \ddots & \ddots & \ddots & \ddots & \vdots \\ 0 & a_q & \cdots & a_2 & \ddots & \ddots & \ddots & a_q & 0 & \vdots \\ \vdots & 0 & a_q & \ddots & \ddots & \ddots & a_2 & \ddots & a_q & 0 \\ \vdots & \ddots & \ddots & \ddots & \ddots & a_2 & a_1 & a_2 & \ddots & a_q \\ \vdots & \ddots & \ddots & \ddots & a_q & \ddots & a_2 & a_1 & a_2 & \vdots \\ \vdots & \ddots & \ddots & \ddots & 0 & a_q & \cdots & a_2 & a_1 & a_2 \\ 0 & \cdots & \cdots & \cdots & \cdots & 0 & a_q & \cdots & a_2 & a_1 \end{bmatrix}}_{n \times n} \quad (1)$$

The related symmetric circulant matrix [21], [22] will be denoted by,

$$\hat{A} = \mathcal{C}(\bar{a}, n) := \underbrace{\begin{bmatrix} a_1 & a_2 & \cdots & a_q & 0 & \cdots & 0 & a_q & \cdots & a_2 \\ a_2 & a_1 & a_2 & \cdots & a_q & 0 & \ddots & \ddots & \ddots & \vdots \\ \vdots & a_2 & a_1 & a_2 & \vdots & a_q & \ddots & \ddots & \ddots & a_q \\ a_q & \cdots & a_2 & a_1 & a_2 & \ddots & \ddots & \ddots & \ddots & 0 \\ 0 & a_q & \cdots & a_2 & \ddots & \ddots & \ddots & a_q & 0 & \vdots \\ \vdots & 0 & a_q & \ddots & \ddots & \ddots & a_2 & \ddots & a_q & 0 \\ 0 & \ddots & \ddots & \ddots & \ddots & a_2 & a_1 & a_2 & \ddots & a_q \\ a_q & \ddots & \ddots & \ddots & a_q & \ddots & a_2 & a_1 & a_2 & \vdots \\ \vdots & \ddots & \ddots & \ddots & 0 & a_q & \cdots & a_2 & a_1 & a_2 \\ a_2 & \cdots & a_q & 0 & \cdots & 0 & a_q & \cdots & a_2 & a_1 \end{bmatrix}}_{n \times n} \quad (2)$$

Throughout this article, variable with a 'hat' such as $\hat{A}$ will be used to represent circulant matrices and their associated eigenvalues.

Note that the two matrices $\mathcal{T}(\bar{a}, n)$ in (1) and $\mathcal{C}(\bar{a}, n)$ in (2) are the same except for the upper right and lower left corners. This fact will be revisited in Section IV.

II. Problem Statement

A. Industrial Cross-Directional Control Processes

An overview of a paper machine showing relative positions of the various actuator arrays and scanning sensor is shown in Figure 1. The wet pulp slurry enters the machine at the left of Figure 1 where it is distributed over a wide area and forced through a gap governed by the slice lip where it is extruded on to a moving wire screen. The remainder of the paper machine first drains then dries the majority of the water from the pulp and a formed sheet of paper is rolled up as illustrated at the right of Figure 1.

The three main properties of interest are weight, moisture, and caliper. The control tuning results shown in Section VI are for two different types of weight control problems - one using a slice lip actuator array and the other a consistency profiling actuator array, which will be described shortly.

The weight per unit area of a sheet of paper, expressed in grams per square meter (gsm) or in pounds per ream is an important factor in the quality of the finished product. Deviations in the paper sheet's weight from its target will affect most other properties [23]. The desired weight targets for papermaking cover a wide range. A sheet of newsprint has a target weight of about 45gsm, a paperback book cover may have a weight of about 300gsm, and cardboard may weigh 450gsm.

CD control of the weight of a paper sheet is accomplished by actuators at the headbox (left side in Figure 1). The function of weight control actuators is to achieve an even distribution of the pulp fibres across the width of the wire belt, despite

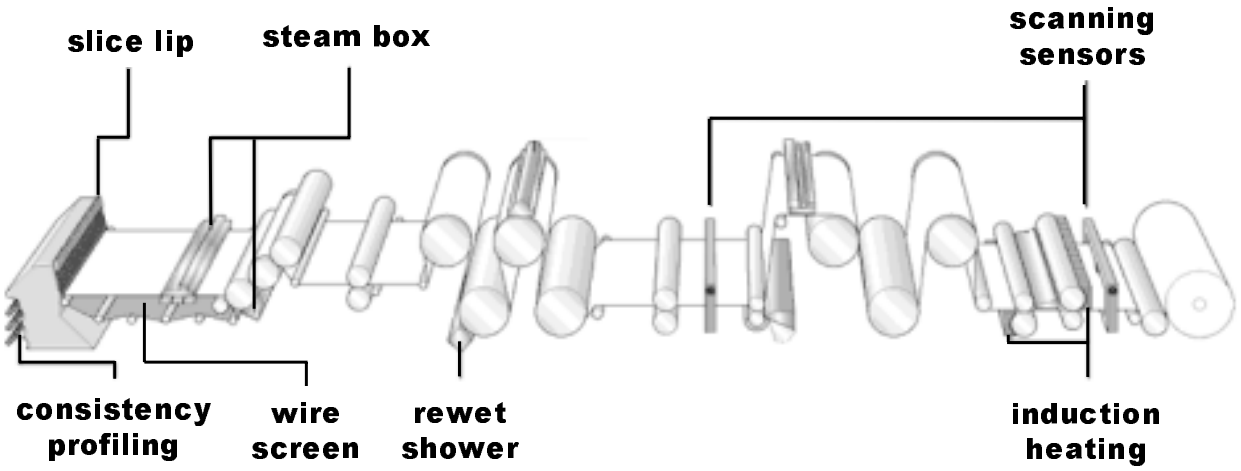

Fig. 1. Wide view of the paper machine showing typical positions of the various actuator arrays and scanning sensor(s). (Artwork courtesy of Honeywell Industry Solutions.)

changing pulp properties. Since the weight control actuators are located the furthest upstream, the dynamics of weight control often require the consideration of a significant dead time component, as the paper sheet must travel through the entire machine before reaching the scanning sensor.

Due to the nature of the raw material, the pulp stock characteristics change over time. The consistency and drainage properties of the delivered stock are kept as constant as possible by the approach system, but variability inevitably occurs. In addition, the flow of the pulp stock through the headbox and on the wire belt can distribute the wood fibres unevenly in the cross-direction. Basis weight profile control is important not only for paper strength reasons, but also due to the fact that a poor quality weight profile will propagate downstream and appear as disturbances in both the moisture and caliper profiles. The control of weight profiles with slice lip actuators and consistency profiling actuators is described in Section VI.

The moisture content of a sheet of paper is a very important factor in determining paper strength [23]. Typical moisture content targets are 5–9% of the total weight of the paper sheet. Overdrying a paper sheet will reduce its strength as the fibres are damaged. An excessively variable moisture profile leads to a variable temperature profile and thus increases the demand on the caliper profiling actuators.

The dewatering and drying of the paper sheet as it passes through the paper machine is very complex and is affected by many factors. The fibre slurry exiting the headbox is approximately 0.5% fibres and 99.5% water. The paper which is wound up on the reel is about 95% fibres and 5% water. The goal of feedback CD control of moisture is to perform the fine control and level a variable moisture profile.

The caliper of a sheet of paper is controlled by feeding the paper sheet through rotating rollers, known as the calendar stack. The pressure that the rolls exert on the paper sheet may be adjusted by locally heating (cooling) one of the rollers. As the temperature of the roller increases (decreases), its diameter also increases (decreases) due to thermal expansion, and thus the pressure on the paper sheet increases (decreases), leading to a decrease (increase) in the paper caliper [24].

Early CD caliper control was implemented through the use of hot and cold air showers on the roller. Modern caliper control is much more efficient and uses induction heating actuators. A high frequency alternating current is used to generate an oscillating magnetic field at the roller surface. The resulting eddy currents near the surface of the roller cause the temperature of the roller to rise, and a local increase in roller diameter with subsequent pressure on the paper sheet.

B. Process Model

The high-level structure of a typical industrial CD control system is illustrated in Figure 2. This structure is discussed in more details in the next section. It is important to note that the computations in a CD control system are organized in two parts. The upper part of the diagram shows controller computations that are performed at the spatial resolution of the actuator profile. Such profiles have 30–300 elements, corresponding to the number of the actuators.

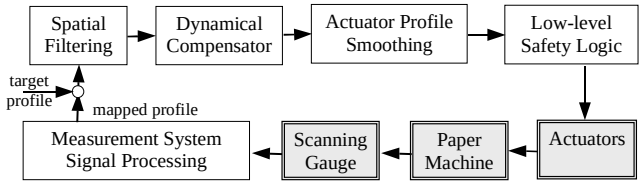

Fig. 2. The flow of information for an industrial cross-directional control system.

The lower part of Figure 2 illustrates the operations involved in processing the signal obtained from the scanning sensor at a much higher spatial resolution with up to 2000 elements. As illustrated in Figure 1, this sensor is mounted on a fixed frame and is scanning back and forth across the paper sheet at a rate of 15–45 seconds per crossing. Because the paper sheet is moving, the scanner actually traces out a zig-zag path on

the sheet. Thus the measurement signal contains both cross-directional information and information regarding the change in the average properties of the sheet – referred to as machine-direction (MD) variability. It is not a trivial problem to separate the measurement signal into its CD and MD components [25], [26]. The industrial system in Figure 2 uses a simple temporal filter in order to prevent transient MD components from distorting the CD profile, and other industrial solutions exist [27]. While removing much of the MD, filtering limits the CD controller to working on disturbances in the CD profile that persist for a long time. However, due to the open-loop transport delay and the first order process dynamics, the CD control system is already limited to disturbances that are much slower than the scanner dynamics [28], [29].

As part of the initial pre-processing and signal conditioning operations in the measurement system this high-resolution measured profile is mapped to the actuator resolution. The mapping is a linear transformation where a single value of the profile error is computed for each actuator as an weighted average of multiple high-resolution profile measurements in the spatial neighborhood of the actuator. Performing all control computations at the actuator resolution corresponds to squaring down of the system, a commonly accepted practice in multivariable process control. More discussion of optimality and achievable performance for the mapped control can be found in [18]. In what follows, the mapping is considered as a fixed part of the measurement system and the controller analysis, design, and tuning are performed for the square system.

The process response to the actuators has both a dynamic and a spatial component. Although the processes described in Subsection II-A use a variety of physical mechanisms, the main features of each of these are captured by a simple mathematical model. The process dynamic and spatial responses are assumed to be separable, and this assumption has been incorporated into the industrial process identification software tool described in [17], [18], [19].

The spatial response of the paper process to the actuator profile is modelled by a convolution of the actuator profile along with the spatial unit impulse response, also known as the CD bump response. Typically the bump response is much narrower than the width of the paper sheet. The dynamics of the CD process response are taken to be first order with deadtime. The deadtime models the transport delay equivalent to the time taken for the paper to travel from the actuators to the scanning sensor. The process model may then be represented as a time domain update equation,

$$y(t) = B \cdot u(t-d) + a \cdot y(t-1), \tag{3}$$

where n is the number of CD actuators, the array $u(t) \in \Re^n$ is the actuator profile at time t, the array $y(t) \in \Re^n$ is the measured paper profile at time t, integer d represents the process deadtime, the scalar a is the open-loop pole of the process, and the constant matrix $B \in \Re^{n\times n}$ contains the spatial response model. The matrix B is taken to be a band-diagonal, symmetric Toeplitz matrix as in (1) with,

$$B = \mathcal{T}(\bar{b}, n), \qquad \bar{b} = [b_1, \ldots, b_{n_b}]^T \tag{4}$$

where usually $n_b \ll n$ for industrial paper machine processes.

The representation in (3) may be written as a transfer matrix,

$$\begin{aligned} y(z) &= G(z)u(z), \\ G(z) &= [1 - a \cdot z^{-1}]^{-1} \cdot z^{-d} \cdot B \end{aligned} \tag{5}$$

where $G(z) \in \mathcal{C}^{n\times n}$, and the Laplace variable z of the $\mathcal{Z}$-transform has the usual meaning as a time shift operator $z^{-1}u(t) = u(t-1)$.

Strictly speaking, the process model in (3) and (5) is correct only if the deadtime is equivalent to an integer multiple of the sample time. In general this will not be the case and modelling a known noninteger deadtime would require an additional (potentially nonminimum phase) zero in the 'true' transfer function. Because of the presence of noninteger deadtime, and due to the fact that the process deadtime may change, uncertainty in the process model dynamics is permitted by the proposed controller design. Model uncertainty and closed-loop robustness are addressed in Subsection III-C below.

C. Industrial Controller Structure

As shown in Figure 2, a typical industrial CD control law has three main components beyond the actuator mapping. These components are spatial decoupling, dynamic compensator, and actuator profile smoothing. The spatial decoupling is implemented as a convolution window similar to the spatial model response in (3). Let $e(t) \in \Re^n$ be the error profile at time t. The output $e_w(t)$ of the spatial decoupling block can be presented in the form

$$e_w(t) = C \cdot e(t), \tag{6}$$

where $C \in \Re^{n\times n}$ is a band-diagonal symmetric Toeplitz 'decoupling matrix' defined in (9) below.

The dynamic compensator, known as a Dahlin controller, is a proportional-integral controller with deadtime compensation, and may be implemented in velocity form as

$$v(t) = (1-\alpha_c)\left[e_w(t) - a_c \cdot e_w(t-1) - \sum_{i=1}^{d_c-1} v(t-i)\right] \tag{7}$$

where the controller tuning is performed by selecting the parameters α_c, a_c, and d_c. Internal model tuning guidelines suggest setting $a_c = a$ and $d_c = d$ according to the process model parameters in (3).

The actuator profile is then updated using the calculation,

$$u(t) = D \cdot [v(t) + u(t-1)], \tag{8}$$

where the constant 'smoothing' matrix D in (8) is again a band-diagonal, symmetric Toeplitz matrix. The matrices C in (6) and D in (8) are respectively,

$$\begin{aligned} C &= \mathcal{T}(\bar{c}, n), \qquad \bar{c} = [c_1, \ldots, c_{n_c}]^T \\ D &= \mathcal{T}(\bar{d}, n), \qquad \bar{d} = [d_1, \ldots, d_{n_d}]^T \end{aligned} \tag{9}$$

using the notation from (1). The smoothing matrix D is further parameterized in terms of a Blackman convolution window filter H such that

$$D = I + \lambda \cdot (H - I) \tag{10}$$

where $0 \leq \lambda < 1$ and n_d defines the width of D in (8), (10), with H being a symmetric Toeplitz matrix,

$$H = \mathcal{T}(\bar{h}, n), \quad \bar{h} = [h_1, \ldots, h_{n_d}]^T \tag{11}$$

where the elements of $\bar{h}$ are defined by a lowpass Blackman window of order n_d normalized such that $h_1 + 2 \cdot h_2 + \ldots + 2 \cdot h_{n_d} = 1$. Consider for example $n_d = 3$ in (11), then $[h_1, h_2, h_3] = [0.3968, 0.2500, 0.0516]$, so that $h_3 + h_2 + h_1 + h_2 + h_3 = 1$.

Note that the actuator profile smoothing operation (8) is responsible for providing the integrator in the control loop. Typically the loop is tuned with $\lambda \approx 0$ such that $D \approx I$ in (8) in order to preserve the closed-loop performance at low frequencies ω. However, we will see in Section V that $D \neq I$ is necessary to guarantee stable closed-loop operation with nonzero model uncertainty.

The feedback controller, (6)–(8) can be written as a transfer matrix,

$$\begin{aligned} u(z) &= K(z)e(z), \\ K(z) &= [I - D \cdot z^{-1}]^{-1} D \cdot c(z) \cdot C \end{aligned} \tag{12}$$

where the constant matrices C and D are defined in (6) and (8)–(11) respectively. The scalar transfer function,

$$c(z) = \frac{(1-\alpha_c)[1 - a_c z^{-1}]}{1 + (1-\alpha_c) \sum_{i=1}^{d_c - 1} z^{-i}} \tag{13}$$

represents the $\mathcal{Z}$-transform of the Dahlin controller in (7).

III. Closed-Loop Requirements

The following specifications must be satisfied for an acceptable industrial control design.

A. Internal Stability

All processes in question are open-loop stable ($0 < a < 1$ in (5)). The feedback controller itself may be marginally stable ($0 < \alpha_c < 1$ and $|\text{eig}(D)| \leq 1$ in (12)), then the requirement of internal stability is equivalent to specifying that the closed-loop transfer matrix,

$$K(z) \left(I + G(z)K(z)\right)^{-1} \tag{14}$$

is stable (analytic for all $|z| \geq 1$ and $z \in \mathcal{C}$) with $K(z)$ in (12) and $G(z)$ in (5).

B. Performance

Cross-directional control is largely a regulation problem and performance is specified by the effect of the output disturbance d_y on the error profile $e = r - y$. Expanding the specification frequency-by-frequency with $d_y(\omega)^T = [d_{y1} e^{i(\omega t + \phi_1)}, \ldots, d_{yn} e^{i(\omega t + \phi_n)}]$ we write,

$$\frac{\|e\|_2}{\|d_y\|_2} < \frac{1}{p}, \qquad \forall\, d_y \in \Omega_l \tag{15}$$

where $p \gg 1$, the norm is defined $\|d_y(\omega)\|_2 := \sqrt{d_y(\omega)^H d_y(\omega)}$ (the superscript H denotes the conjugate transpose). In an ideal design, the set Ω_l would contain all significant disturbances in the system. However, in practice a performance specification such as (15) can only be enforced for controllable disturbances[1], typically at low temporal frequencies ω (see for example [30], [31]). The form of the performance specification (15) allows for additional flexibility according to the directionality of the disturbance d_y. The necessity of this was the central issue of [32] and will be demonstrated in Section V below.

C. Robust Stability Margin

The parameters of the process model $G(z)$ in (5) are identified from input/output process data, and uncertainty in the model is unavoidable. CD processes are somewhat unusual control systems in that, due to the ill-conditioning, there is a sign uncertainty of the steady-state gain ($\omega = 0$) in certain input directions of the process [32], [33], [1]. This form of model uncertainty may be captured with an additive matrix perturbation,

$$G_p(z) = G(z) + \delta G(z) \tag{16}$$

Then designing the controller $K(z)$ such that the closed-loop is internally stable (condition (14)) and

$$\max_{d_y \neq 0} \frac{\|u\|_2}{\|d_y\|_2} = \bar{\sigma}(K[I + GK]^{-1}) < \frac{1}{\beta} \tag{17}$$

where $\bar{\sigma}(\cdot)$ denotes the maximum singular value, provides a robust stability margin of β to additive matrix perturbations. In other words, the closed-loop is robustly stable for all processes described by (16) with uncertainty given by a stable perturbation bounded as,

$$\|\delta G(z)\|_\infty \leq \beta \tag{18}$$

D. Low-Order Controller

Low-order controllers are preferred over high-order. From (7) or (13) it is evident that the temporal order of the controller is determined by d_c which typically is set equal to the process model dead time d in (3), (5). The spatial order of the controller[2] is defined by the number of nonzero off-diagonal elements n_c and n_d respectively for the system matrices C and D in (9). The low spatial order requirement is then to ensure that

$$n_c, n_d \ll n \tag{19}$$

in (9) where n is the dimension of the matrices $C, D \in \Re^{n \times n}$.

IV. Two-Dimensional Frequency Domain

A straightforward approach to the above problem requires dealing with a multivariable feedback control system that will have up to $n = 300$ inputs and outputs. However, to address this problem directly is difficult if not intractable. By appealing

[1]Sometimes a high-performance low-frequency specification such as (15) will be accompanied by a looser limit $p < 1$ that must be satisfied for *all* output disturbances d_y with $\|d_y\|_2 < \infty$. This is accomplished indirectly since satisfying the robust stability condition (17) automatically satisfies (15) with $p = \beta / (\beta + \|G(z)\|_\infty)$ for all such bounded d_y.

[2]A distributed controller, implemented with a low spatial order is alternatively referred to as "localized control" [34], [35].

to the structure of the specified system, we will approach the design through a related problem that offers many advantages.

Section II has presented a process model and feedback controller that are each linear, time-invariant, and *almost* spatially-invariant. The convenience of the linear, time invariant (LTI) approximation is that it permits the use of the temporal frequency domain in the analysis and design of control systems. Recent work on linear, spatially-invariant (LSI) control systems [34], [36], [37], [32], [33] has exploited the LSI property to a similar advantage in the spatial frequency domain. The use of spatially-invariant process models in cross-directional control was introduced in [4] where a thorough development of spatial frequencies may be found. This approach has been used subsequently in an analogous but somewhat different manner in [2] and more such examples may be found in [5], [38], [39].

As seen in Section II, the form of the model implies that the process response is the same for each actuator, except that it is shifted accordingly in the cross-direction. The spatial invariance is disrupted by the edges of the paper sheet where the response is truncated. The same kind of structure is present in the industrial CD controller as well. The effect of such spatial boundary effects in distributed control systems is currently the subject of active research (see [40], [41]).

The simplest way to obtain a spatially-invariant system in our case is to impose spatially periodic boundary conditions on the process model and controller as in [2], [32]. Physically speaking, this approximation corresponds to manufacturing a *tube* of paper, rather than a flat sheet. Mathematically, this is achieved by replacing the symmetric Toeplitz matrices $\{B, C, D\}$, in (4), (5), (9), and (12) with symmetric *circulant* matrices $\{\hat{B}, \hat{C}, \hat{D}\}$. For example, the circulant extension $\hat{B}$ of the Toeplitz B in (4) is given by the notation in (2)

$$\hat{B} = \mathcal{C}(\bar{b}, n) \tag{20}$$

where $\bar{b} = [b_1, \ldots, b_{n_b}]^T$ in (4) and typically $n_b \ll n$ for the problem at hand. The difference between the circulant and Toeplitz matrices is given by,

$$\delta B \quad = \quad \hat{B} - B, \tag{21}$$

so that δB contains the 'ears' of the circulant matrix, as shown in Figure 3.

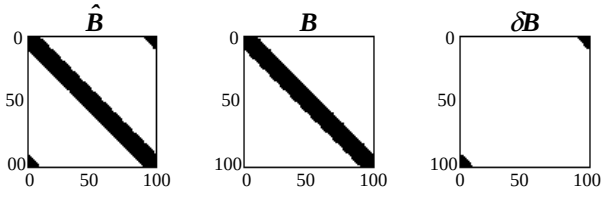

Fig. 3. Non-zero elements of a banded symmetric circulant matrix $\hat{B}$ in (20), the associated band-diagonal symmetric Toeplitz symmetric matrix B in (4), and the difference described by the 'ears' in $\delta B = \hat{B} - B$ in (21).

The advantage of this approximation is evident from noting that every symmetric circulant matrix (of the same size) may be diagonalized by the real valued Fourier matrix, given by

$$F(j,k) \quad = \quad \begin{cases} \sqrt{\frac{1}{n}}, & j = 1 \\ \sqrt{\frac{2}{n}} \cdot \sin[(k-1)\nu_j], & j = 2, \ldots, q \\ \sqrt{\frac{2}{n}} \cdot \cos[(k-1)\nu_j], & j = q+1, \ldots, n \end{cases} \tag{22}$$

where $q = (n+1)/2$ if n is odd and $q = n/2$ if n is even [21], [42]. The j^{th} row of F contains the j^{th} spatial harmonic and has frequency,

$$\nu_j \quad = \quad 2\pi(j-1)/n \tag{23}$$

Consider the process model and controller transfer matrices with symmetric circulant coefficients $\{\hat{B}, \hat{C}, \hat{D}\}$ in the place of truncated Toeplitz matrices $\{B, C, D\}$ in (5) and (12),

$$\begin{aligned} \hat{G}(z) &= [1 - a \cdot z^{-1}]^{-1} \cdot z^{-d} \cdot \hat{B}, \\ \hat{K}(z) &= [I - \hat{D} \cdot z^{-1}]^{-1} \hat{D} \cdot c(z) \cdot \hat{C} \end{aligned} \tag{24}$$

Then pre- and post-multiplying the process model $\hat{G}(z)$ and $\hat{K}(z)$ by the real Fourier matrix $F(\cdot)F^T$, we can simultaneously diagonalize the process model and controller,

$$\begin{aligned} F \cdot \hat{G}(z) \cdot F^T &= \text{diag}\{\hat{g}(\nu_1, z), \ldots, \hat{g}(\nu_n, z)\}, \\ F \cdot \hat{K}(z) \cdot F^T &= \text{diag}\{\hat{k}(\nu_1, z), \ldots, \hat{k}(\nu_n, z)\} \end{aligned} \tag{25}$$

where the SISO transfer functions on the diagonal of (25) are

$$\begin{aligned} \hat{g}(\nu_j, z) &= \frac{\hat{b}(\nu_j) \cdot z^{-d}}{1 - az^{-1}}, \\ \hat{k}(\nu_j, z) &= \frac{\hat{c}(\nu_j)\hat{d}(\nu_j)}{1 - \hat{d}(\nu_j)z^{-1}} \cdot c(z) \end{aligned} \tag{26}$$

and the spatial frequencies take the values $\nu_j \in \{\nu_1, \ldots, \nu_n\}$. Note that the gain $\hat{b}(\nu_j)$ of the process model $\hat{g}(\nu_j, z)$ changes with respect to spatial frequency ν_j. The controller $\hat{k}(\nu_j, z)$ has its gain and one of its poles being functions of spatial frequency.

The real Fourier matrix F in (22) is unitary so that $F^{-1} = F^T$ and therefore the singular values of the symmetric circulant system are equivalent to the absolute value of the eigenvalues in (25). Figure 4 illustrates the singular values of a typical cross-directional process model as a function of spatial and temporal frequencies.

High-frequency gain roll-off is a familiar feature of dynamic systems. Figure 4 illustrates the typical case for cross-directional control systems, where the gain rolls-off for high spatial and temporal frequencies. In multivariable terms, this is (correctly) referred to as an ill-conditioned system due to the fact that the smallest singular values of the plant model - given by the magnitude of the eigenvalues $|\hat{g}(\nu_j, e^{i\omega})|$ in (26) - approach zero relative to the largest singular values. The advantage of the two-dimensional frequency domain interpretation is in the fact that frequency domain methods are very well-developed for addressing gain roll-off. In particular, the trade-off of performance and robustness specifications at low and high temporal frequencies respectively is central to traditional loop shaping controller design techniques (for example [30], [31]). This concept has been extended to the two-dimensional frequency domain in [32], [33]. Two-dimensional loop shaping

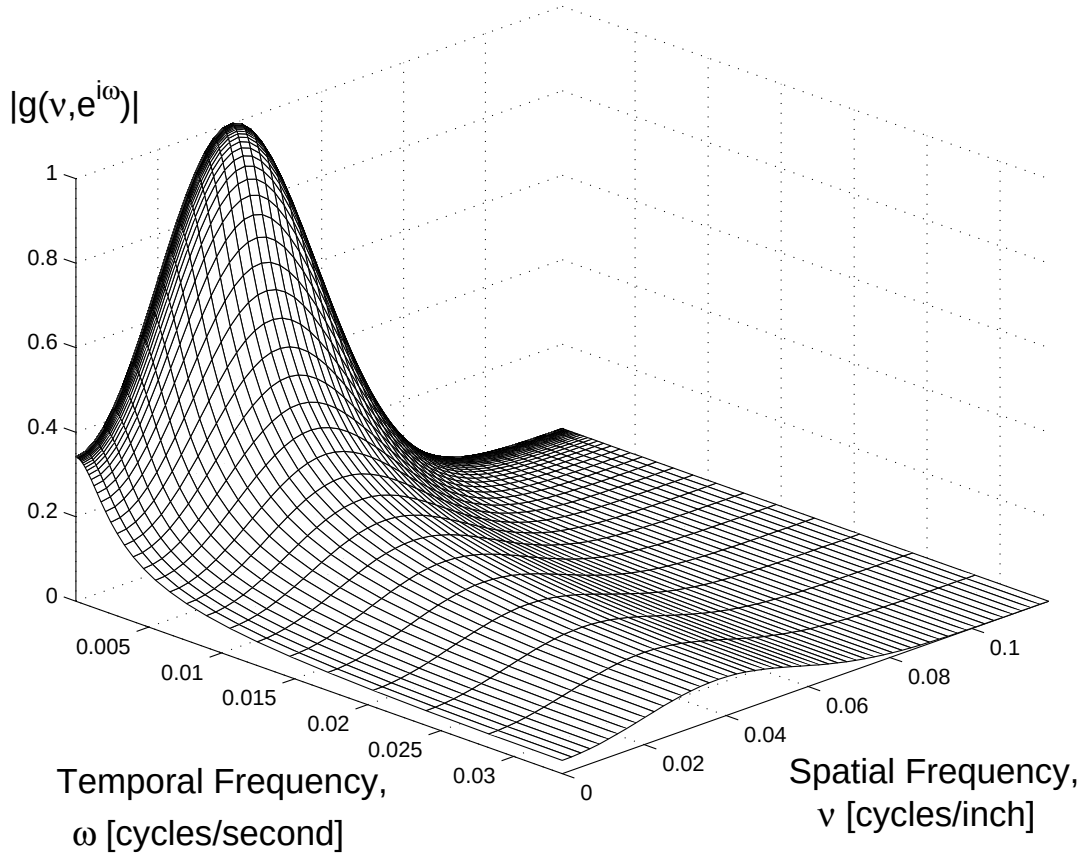

Fig. 4. Surface plot of the two-dimensional frequency response $|\hat{g}(\nu_j, e^{i\omega})|$ in (26) of the open-loop process model for the slice lip process (the same process model is also illustrated in Figure 7).

approaches controller design for processes modelled such as $\hat{g}(\nu_j, e^{i\omega})$ in (26) by applying the performance and robustness requirements at locations of high and low process gain respectively. For typical model responses for cross-directional process such as illustrated in Figure 4, this will result in the application of performance specifications at low spatial and temporal frequencies and robustness specifications at high spatial and temporal frequencies. The two-dimensional loop shaping technique allows to easily design a controller for the ill-conditioned process model, and is used in the following Section.

V. Constructive Controller Design

A. Restatement of Closed-Loop Requirements in the Two-Dimensional Frequency Domain

The requirement of internal stability is satisfied for the circulant system composed of $\hat{G}(z)$ and $\hat{K}(z)$ in (24) if and only if each member of the diagonalized system is stable. Since each $\hat{g}(\nu_j, z)$ in (26) is stable and each $\hat{k}(\nu_j, z)$ is stable or marginally stable in (26), then internal stability requires each transfer function,

$$\frac{\hat{k}(\nu_j, z)}{1 + \hat{g}(\nu_j, z)\hat{k}(\nu_j, z)} \tag{27}$$

to be stable for each spatial frequency $\nu_j \in \{\nu_1, \ldots, \nu_n\}$.

The closed-loop performance is stated in terms of the disturbance attenuation analogous to (15), and by writing the sensitivity transfer matrix

$$\left| \frac{1}{1 + \hat{g}(\nu_j, e^{i\omega})\hat{k}(\nu_j, e^{i\omega})} \right| < \frac{1}{p(\nu, \omega)} \tag{28}$$

where satisfying (28) for $p(\nu, \omega) \gg 1$ indicates good performance (disturbance attenuation) at frequencies $\{\nu, \omega\}$.

We will characterize the closed-loop performance in terms of two frequencies indicating the closed-loop bandwidth at which 90% of disturbances are attenuated. The quantity ν_{90} is defined as the spatial frequency below which (28) is satisfied on the ν-axis for $p(\nu, 0) = 10$. The quantity ω_{90} is defined as the temporal frequency below which (28) is satisfied on the ω-axis for $p(0, \omega) = 10$.

To achieve a robust stability margin analogous to (17), we will design $\hat{k}(\nu_j, z)$ for internal stability (condition (27)) and

$$\left| \frac{\hat{k}(\nu_j, e^{i\omega})}{1 + \hat{g}(\nu_j, e^{i\omega})\hat{k}(\nu_j, e^{i\omega})} \right| < \frac{1}{\beta} \tag{29}$$

for all frequencies $\nu_j \in \{\nu_1, \ldots, \nu_n\}$ and $\omega \in [\pi, \pi]$. Note that satisfying condition (29) will lead to a stable closed-loop for any plant $G_p(z) = \hat{G}(z) + \delta G(z)$ with perturbation $\delta G(z)$ stable and bounded as in (18). The transfer matrices $\delta G(z)$ and $G_p(z)$ are *not* restricted to be symmetric circulant matrices.

To achieve a controller with a low spatial order requires the coefficients $\hat{c}(\nu_j)$ and $\hat{d}(\nu_j)$ of $\hat{k}(\nu_j, z)$ in (26), to satisfy

$$\begin{aligned} \hat{c}(\nu_j) &= c_1 + 2 \cdot \sum_{i=2}^{n_c} c_i \cdot \cos[(i-1) \cdot \nu_j], \qquad n_c \ll n \\ \hat{d}(\nu_j) &= d_1 + 2 \cdot \sum_{l=2}^{n_d} d_l \cdot \cos[(l-1) \cdot \nu_j], \qquad n_d \ll n \end{aligned} \tag{30}$$

where the coefficients $\{c_1, \ldots, c_{n_c}\}$ and $\{d_1, \ldots, d_{n_d}\}$ are the weights of the convolution windows corresponding to $\hat{c}$ and $\hat{d}$ in the symmetric circulant matrices $\hat{C}$ and $\hat{D}$ in the controller $\hat{K}(z)$ in (24).

B. Two-Dimensional Loop Shaping Design Considerations

As mentioned above, Figure 4 illustrates the typical case for process models of cross-directional control systems. The gain of the open-loop process $|\hat{g}(\nu_j, e^{i\omega})|$ is large for low spatial and temporal frequencies $\{\nu, \omega\}$ and rolls-off for high spatial and temporal frequencies $\{\nu, \omega\}$. This re-interpretation of the ill-conditioning facilitates the extension of the familiar loop-shaping techniques in temporal frequency domain to the two-dimensional systems at hand.

In the broad sense, loop shaping design techniques are the design of a feedback controller in terms of the closed-loop frequency response under the requirement that closed-loop stability is maintained. These techniques are particularly well-suited for handling high-frequency gain roll-off. There exist well-known open-loop approximations to closed-loop design requirements.

Qualitatively speaking, the performance specification (condition (28)) may be satisfied for a closed-loop stable system, by designing $|\hat{k}(\nu_j, e^{i\omega})|$ to be large at those frequencies $\{\nu_j, \omega\}$ where $|\hat{g}(\nu_j, e^{i\omega})|$ is large and the relative uncertainty is small. The robustness of the closed-loop (condition (29)) is a matter of designing $|\hat{k}(\nu_j, e^{i\omega})|$ to be small at those spatial and temporal frequencies $\{\nu_j, \omega\}$ where $|\hat{g}(\nu_j, e^{i\omega})|$ is small and/or the relative uncertainty is large.

More specifically, for the problem at hand, the closed-loop nominal stability (condition (27)) for each of the spatial frequency modes ν_j is achieved with the parameters of the controller $\hat{k}(\nu_j, z)$ in (13), (26) satisfying:

$$\begin{aligned} a_c &= a, \quad d_c = d, \quad 0 < \alpha_c < 1 \\ 0 &\leq \hat{d}(\nu_j) \leq 1, \\ \hat{c}(\nu_j) &= \frac{\hat{b}(\nu_j)}{\hat{b}(\nu_j)^2 + \hat{r}(\nu_j)}, \qquad \hat{r}(\nu_j) \geq 0 \end{aligned} \tag{31}$$

where the scalars a, d and the spectrum $\hat{b}(\nu_j)$ are model parameters from $\hat{g}(\nu_j, z)$ in (26). The constant α_c and the spectra $\hat{d}(\nu_j)$ and $\hat{r}(\nu_j)$ are to be designed. To demonstrate that (31) will lead to a stable closed-loop, substitute the parameters in (31) into the controller $\hat{k}(\nu_j, z)$ in (13), (26), then together with $\hat{g}(\nu_j, z)$ in (26), it is straightforward to show that the poles of the transfer function in (27) are inside the unit circle (see [33] for details). This leaves us free to shape the two-dimensional frequency response of the closed-loop system for conditions (28), (29), and (30) via the design parameters α_c, $\hat{d}(\nu_j)$ and $\hat{r}(\nu_j)$ in (31).

The proposed design approaches the problem as a two-step synthesis (once along the ω-axis and once along the ν-axis), followed by a full analysis of the two-dimensional system.

Temporal Design

In practice, for spatial frequency $\nu_0 = 0$ in (23) we will have an acceptable model gain $\hat{g}(\nu_0, z)$ in (26) along the temporal frequency ω-axis when $\hat{b}(\nu_0)$ in (26) is large. Therefore the design of the controller $\hat{k}(\nu_0, z)$ in (26) along the ω-axis can proceed using classical SISO design techniques for dynamic systems. Internal model control (IMC) considerations [43] recommend the Dahlin controller be designed with parameters $a_c = a$, $d_c = d$, the pole providing integral action with $\hat{d}(\nu_0) = 1$, and controller gain $\hat{c}(\nu_0) = 1/\hat{b}(\nu_0)$ (see Spatial Design below). For these tuning parameters, the temporal sensitivity function in (28) is given at spatial frequency $\nu_0 = 0$ by,

$$\begin{aligned} \hat{s}(\nu_0, z) &:= \frac{1}{1 + \hat{g}(\nu_0, z)\hat{k}(\nu_0, z)} \\ &= \frac{1 - \alpha_c z^{-1} - (1 - \alpha_c) z^{-d}}{1 - \alpha_c z^{-1}} \end{aligned} \tag{32}$$

and denote the maximum magnitude of the sensitivity function as,

$$M_s := \max_{\omega} |\hat{s}(\nu_0, e^{i\omega})| \tag{33}$$

The remaining tuning parameter α_c is to be designed such that the closed-loop is acceptably fast with a target limit on the peak of the sensitivity function M_s in (33).

In order to simplify the tuning (often done manually), a rule of thumb was developed for field personnel to compute the value of α_c that would approximately result in the desired closed-loop frequency response. The value of M_s in (33) was leastsquares fit to an affine combination of the dead time d and the tuning parameter α_c in (32). This relationship was made constructive by solving the least squares fit for the tuning parameter,

$$\alpha_c = -0.6935 \cdot M_s + 0.0322 \cdot d + 1.6184 \tag{34}$$

where for CD control the target peak of the sensitivity function is typically set to $M_s = 1.2$, thus corresponding to a limit on the magnification of disturbances by $+20\%$ at a (typically) mid-range frequency in the ω-domain[3].

Spatial Design

The spatial design step is concerned with the ν-axis (with temporal frequency $\omega = 0$). The basic goal of the spatial tuning is to successfully trade off performance (28) and robust stability (29) while maintaining the spatial order of the controller, n_c and n_d in (30), to be small.

[3]An additional advantage is that the free parameter α_c of a Dahlin controller such as in (7) or (13) may be tuned for a desired closed-loop response by a simple hand-calculation (34). This is useful as a rule of thumb for field personnel when faced with an immediate tuning problem.

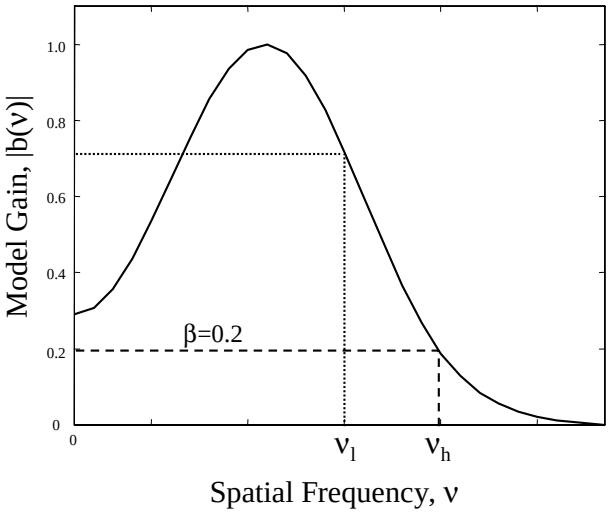

Fig. 5. Illustration of the definition of the low spatial frequency limit ν_l where $|\hat{b}(\nu_l)| = \sqrt{2}/2$ and the high spatial frequency limit ν_h where $|\hat{b}(\nu_h)| = \beta$ for $\beta = 0.2$ in terms of the steady-state model gain in (26). (This curve was taken from the $\omega = 0$ axis of the surface plot of the example in Figure 4.)

As mentioned in Subsection II-C, the smoothing operation has only two degrees of freedom. We initially set the order of the Blackman window to be the smallest allowed with $n_d = 2$. Setting the constant to be small $\lambda = 0.01$ then allows the controller pole $\hat{d}(\nu_j)$ in (26) to be computed as a function of spatial frequency by (10), (30) with coefficients,

$$d_l = \begin{cases} 1 + \lambda \cdot (h_1 - 1) & l = 1 \\ \lambda \cdot h_l & l = 2, \ldots, n_d \end{cases} \tag{35}$$

where the scalars h_l with $l = 1, \ldots, n_d$ are defined by a lowpass Blackman window of order n_d as described in (11).

For the majority of CD processes, a robust stability margin $\beta = 0.2 \cdot \left\| \hat{G}(z) \right\|_\infty$ has proven to be acceptable. Then, given smoothing spectrum $\hat{d}(\nu_j)$ and Dahlin controller parameters α_c, a_c, d_c, it remains to design the controller gain $\hat{c}(\nu_j)$ with respect to performance (28) and robust stability (29).

As with traditional loop shaping, these requirements do not conflict since they are applied at different spatial frequencies. At low spatial frequencies ν, the process gain $\hat{b}(\nu_j)$ is large relative to the model uncertainty β and the closed-loop performance is important, while at high spatial frequencies ν, the process gain $\hat{b}(\nu_j)$ is small relative to the model uncertainty β and robustness is more important.

In characterizing the design, it is useful to define two spatial frequency limits as illustrated in Figure 5. The low frequency limit ν_l was developed in practical cross-directional control to be the frequency at which the model gain rolls off to $\sqrt{2}/2$ of its maximum value[4],

$$|\hat{b}(\nu_l)| = \frac{\sqrt{2}}{2}, \tag{36}$$

[4]Strictly speaking the spatial frequency array is defined only on the discrete values $\{\nu_1, \ldots, \nu_n\}$, and interpolation is used to define the values ν_l and ν_h in (36) and (37). This interpolation is of little practical importance as these frequencies are used as target values.

and the minimum requirement in the papermaking industry is that a cross-directional controller will remove 'all' steady-state variability with a spatial frequency smaller than ν_l in (36). This limit will be used constructively in the controller synthesis algorithm below.

The high spatial frequency limit ν_h is derived as the lowest frequency for which the process model gain is smaller than the magnitude of the uncertainty β in (18) or (29),

$$|\hat{b}(\nu_h)| = \beta \tag{37}$$

The high frequency ν_h defines the spatial frequency limit beyond which we cannot guarantee any performance improvement with a feedback controller due to the uncertainty being larger than the model gain [5].

In [33] the detailed calculation of the array $\hat{r}(\nu_j)$ is computed in terms of the process gain spectrum $\hat{b}(\nu_j)$, but is not repeated here. It is enough to understand that typically,

$$\begin{aligned} \text{performance:} \quad & \hat{r}^*(\nu_j) \to 0 \quad \text{for low } \nu_j \\ \text{robust stability:} \quad & \hat{r}^*(\nu_j) > 0 \quad \text{for high } \nu_j \end{aligned} \tag{38}$$

Then the target controller gain is constructed such that

$$\hat{c}^*(\nu_j) = \frac{\hat{b}(\nu_j)}{\hat{b}(\nu_j)^2 + \hat{r}^*(\nu_j)} \tag{39}$$

In general, the controller gain designed frequency-by-frequency such as $\hat{c}^*(\nu_j)$ in (39) will not satisfy the requirement of a low spatial order (30).

The synthesis step outlined in (38) and (39) is then followed by an order reduction operation where a low-order spectrum $\hat{c}(\nu_j)$ is fit to the target high-order spectrum $\hat{c}^*(\nu_j)$ in (39) (compare Theorem 4 in [32]). We expand the spectrum and compute the first n_c terms,

$$c_i = \frac{1}{n} \sum_{j=1}^{n} \hat{c}^*(\nu_j) \cdot \cos[(i-1) \cdot \nu_j], \qquad i = 1, \ldots, n_c \tag{40}$$

where n_c is the spatial order of $\hat{C}$ in (30). Equations (38)–(40) outline the "synthesis" routine referred to in Subsection V-C below.

Finally, the spectrum corresponding to the reduced-order decoupling operator is created using,

$$\hat{c}(\nu_j) \quad = \quad c_1 + 2 \cdot \sum_{i=2}^{n_c} c_i \cdot \cos[(i-1) \cdot \nu_j], \tag{41}$$

Analysis

The above design has resulted in a distributed feedback controller with low spatial order $n_c, n_d \ll n$ in (30). It remains to verify that the robust stability condition (29) is satisfied for the maximum over all spatial and temporal frequencies $\{\nu, \omega\}$. The closed-loop performance of the system is presented in terms of the performance frequencies ν_{90} and ω_{90} as described in Subsection V-A above.

C. Controller Tuning Algorithm

This section contains an overview of the main components of the algorithms for two-dimensional loop shaping for cross-directional controller tuning.

Phase I: Initialization

1) Given an identified model in (3) compute the model parameters $\hat{b}(\nu_j)$, a and d in (26).
2) Set controller parameters $a_c = a$, $d_c = d$ in (7) and initialize α_c with target sensitivity function peak $M_s = 1.2$ in (34).
3) Initialize low and high limits $\lambda_l = 0.0005$ and $\lambda_h = 0.06$. Initialize $\lambda = (\lambda_l + \lambda_h)/2$ and the Blackman filter order $n_d = 2$ in (35) and compute $\hat{d}(\nu_j)$ in (26), (30).
4) Initialize target stability margin $\beta = 0.2$ and controller spatial order $n_c = 10$. (This spatial order has been found to be large enough to cover practical cases.)
5) Call "synthesis" routine (38)–(40) to compute $\{c_1, \ldots, c_{10}\}$.
6) Reduce the value of n_c such that the sequence of coefficients $\{c_1, \ldots, c_{n_c}\}$ changes sign at most once.
7) Using the model gain $\hat{b}(\nu_j)$ computed in Phase I, calculate the low and high spatial frequency limits ν_l in (36) and ν_h in (37).
8) Define the target frequency $\nu^* = (\nu_l + \nu_h)/2$ and tolerance $\epsilon = (\nu_h - \nu_l)/20$.

Phase II: Tuning Iteration

1) Set $\lambda = (\lambda_l + \lambda_h)/2$ in (35) and call "synthesis" routine (38)–(40) to compute $\{c_1, \ldots, c_{n_c}\}$.
2) Compute ν_{90} on the ν-axis ($\omega = 0$) as the highest spatial frequency for which the performance condition (28) is satisfied for $p(\nu, 0) = 10$.
3) Is $|\nu_{90} - \nu^*| < \epsilon$? If YES, then goto 6. If NO, then continue.
4) If $\nu_{90} > \nu^*$, then set $\lambda_l = \lambda$ and goto 1.
5) If $\nu_{90} < \nu^*$, then set $\lambda_h = \lambda$ and goto 1.
6) Extract the controller parameters $\{c_1, \ldots, c_{n_c}\}$, $\{d_1, \ldots, d_{n_d}\}$, α_c, a_c, d_c.
7) Verify the closed-loop stability of the associated truncated Toeplitz system.
8) Transfer the controller parameters to the working cross-directional control system.

Phase III: (Optional) Direct Modification by the User

1) Via the graphical interface, the user is permitted to change: the spatial order of the controller decoupling n_c, or actuator profile smoothing n_d in (30), the target stability margin β in (29), and the values of λ in (35) and α_c in (13) and (26).
2) Call "synthesis" routine (38)–(40) to compute $\{c_1, \ldots, c_{n_c}\}$.
3) Check that $\nu_l < \nu_{90} < \nu_h$.
4) If NO, then a warning is presented to the user to return to 1.
5) Extract the controller parameters $\{c_1, \ldots, c_{n_c}\}$, $\{d_1, \ldots, d_{n_d}\}$, a_c, d_c.
6) Verify the closed-loop stability of the associated truncated Toeplitz system.
7) Transfer the controller parameters to the working cross-directional control system.

VI. Two Industrial Applications

A. System 1: A Closed-Loop Unstable Slice Lip System

The data in this work are taken from a paper machine at an American paper mill that had been experiencing closed-loop instability problems [15]. Certain modes of closed-loop instability in CD control of paper machines can be very slow to develop, being unnoticeable following the controller tuning. This particular paper machine had been tuned such that it appeared to be stable and producing good paper. However, while in closed-loop, a high spatial frequency component in the actuator profile would steadily increase in magnitude and within one day of operation the actuators would reach their limits. Figure 6 illustrates the familiar mode of instability referred to by papermakers as 'actuator picketing' due to the picket fence appearance of the actuator profile. At this point, the machine operators would take the system off-line, reset the actuator profile to zero, and start over. The system would perform well initially, but the same instability would eventually reappear. Figure 6 illustrates a snapshot of the closed-loop system with the picketing instability.

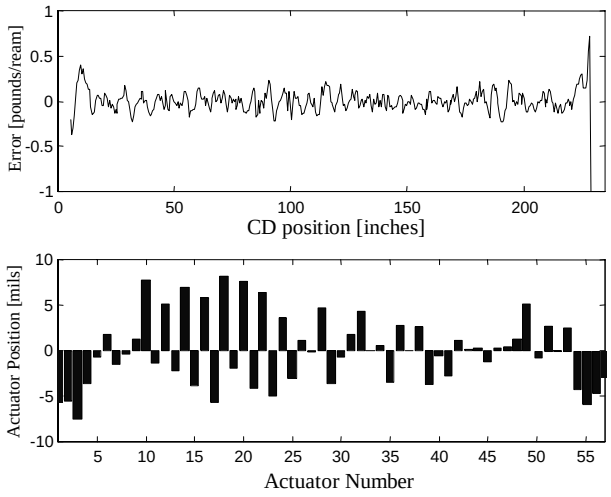

Fig. 6. Snapshot of the drifting, picketing actuator profile instability for the slice lip system.

The use of a slice lip is the traditional method of controlling the CD profile of basis weight of a paper sheet. The slurry exits the headbox through an opening which is as wide as the paper machine (up to 11m) but only 1cm–2cm tall for fine paper and 4cm–6cm tall for linerboard. The amount of pulp exiting the headbox is controlled by locally changing the height of this opening by bending its flexible upper lip. A taller opening is used to allow more pulp on to the wire thus increasing the amount of fibres at that location and increasing the basis weight.

The bending of this upper lip is controlled by an array of force actuators distributed along its length. A typical slice

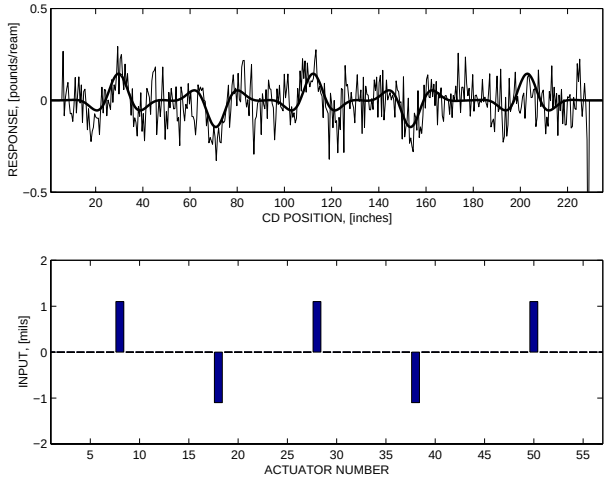

Fig. 7. The open-loop steady-state spatial response of the directory grade paper sheet to changes in the slice lip actuators.

lip installation has $n = 50$ of such actuators in the array, but there exist installations with $n = 118$ or more slice lip actuators. The actuator spacing is quite variable depending on the installation and is anywhere from 7.0cm to 20cm. Modern slice lip actuator dynamics are very fast compared with the scan time. The process dynamics are thus dominated by the sensor filtering and the dead time due to the transport delay from the actuators to the scanning sensor.

The slice lip itself is quite expensive, and much care is taken to prevent damaging it due to excessive flexing and bending. Depending on the lip material, each actuator has a range of at most 0.17mm-0.75mm. The industrial controller contains many safety interlocks and an actuator setpoint profile is prevented from violating the bending constraints specified for the slice lip. However, an actuator setpoint profile as illustrated in Figure 6 is cause for concern as the increased bending will shorten the life of the lip.

The paper machine in question was producing a light 'directory grade' paper sheet, used for the pages of a telephone directory. The target weight of the paper sheet was between 18–21 pounds/ream, where a ream is a unit of area equal to 3000 square feet. The paper profiles are measured by a scanning sensor with a scan time of 25 seconds. In this example, the scanning gauge measured at $m = 456$ evenly-spaced locations across the width of the paper sheet, and the mapped profile has dimension of $n = 54$ corresponding to the number of working actuators.

The quantitative analysis of the instability problem described qualitatively above, begins with the identification of a process model. Following an open-loop 'bump test', the process model was identified from input-output data using the industrial software [17]. The parameters of the model (3) representing the slice lip process are displayed in Table I. Using the data in Table I, a circulant extension to the Toeplitz process model was computed as in (20) and the two-dimensional frequency response $\hat{g}(\nu_j, z)$ of the open-loop system was computed as shown in (26) and is illustrated in Figure 4. Note that the gain of the process is small for high frequencies – both spatially and temporally.

The analysis and design of this cross-directional control system proceeds in terms of the two-dimensional frequency domain requirements (27)–(30). Due to space considerations, we will concentrate the description of the two-dimensional loop shaping on the robust stability requirement (29). As shown by the closed-loop instability problems this is the most relevant issue with regard to this slice lip system.

Condition (29) describes a requirement on the closed-loop system that must be satisfied in order for the system to maintain robust stability in spite of model uncertainty. It is well known from traditional loop shaping for dynamical systems (e.g. [30], [31]) that such closed-loop conditions are approximated by open-loop conditions when the loop gain is very high or very low. We borrow that approximation here in order to provide an intuitive, conceptual description of the

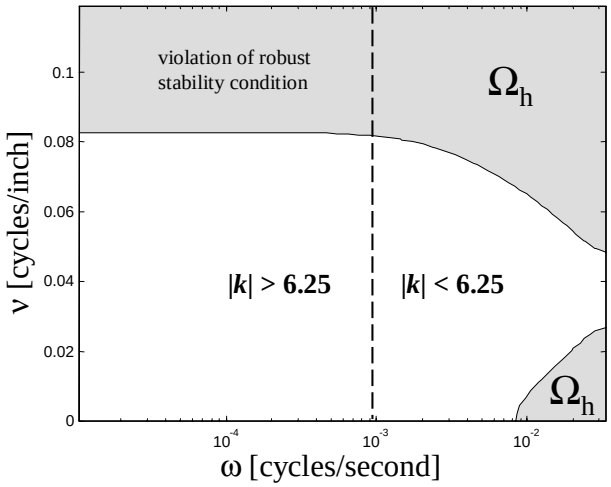

Fig. 8. The open-loop stability margin condition (42) is violated at low temporal frequencies ω and high spatial frequencies ν for the original (decentralized) controller in Table II for the slice lip system.

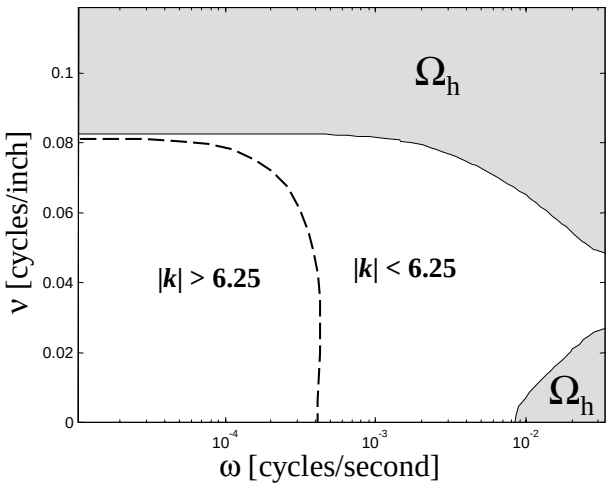

Fig. 9. The dashed line shows the $|\hat{k}(\nu_j, e^{i\omega})| = 6.25$ contour in $\omega\nu$ of the controller in Table II designed by two-dimensional loop shaping to satisfy the stability margin condition (29) for the slice lip system.

Model parameter	Symbol	Identified value
number of actuators	n	54
spatial order	n_b	6
spatial response	$\bar{b}$	[1.8987, 0.7580, -0.5827, -0.4732, -0.0573, 0.0272] $\times 10^{-2}$
dead time	d	3
pole	a	0.8311

TABLE I
PROCESS MODEL PARAMETERS (3)–(5) FOR THE SLICE LIP SYSTEM.

Controller parameter	Symbol	Original tuning	Loop shaping tuning
decoupling spatial order	n_c	1	3
decoupling convolution	$\bar{c}$	[57.1599]	[13.6440, 4.4919, -1.9652]
smoothing spatial order	n_d	1	4
smoothing convolution	$\bar{d}$	[1]	[0.9860, 0.0046, 0.0020, 0.0004]
internal model pole	a_c	0.7408	0.7344
internal model dead time	d_c	4	2
alpha	α_c	0.8465	0.8142

TABLE II
CONTROLLER TUNING PARAMETERS (6)–(9) FOR THE SLICE LIP SYSTEM.

controller tuning problem and its resolution.

It can be shown that, for a nominally stable closed-loop system, a necessary condition for the satisfaction of the closed-loop condition (29) is provided by the open-loop condition,

$$\begin{aligned} |\hat{k}(\nu_j, e^{i\omega})| &< 6.25, \\ \Rightarrow \quad \beta(\nu_j, \omega) &> 0.08, \end{aligned} \tag{42}$$

for all $\{\nu_j, \omega\} \in \Omega_h$ defined as

$$\Omega_h := \{\{\nu, \omega\} : |\hat{g}(\nu_j, e^{i\omega})| < 0.08\} \tag{43}$$

This set is illustrated as the shaded areas in Figures 8 and 9.

The values of the parameters in the original tuning of the feedback controller are indicated in Table II. Since it is completely decentralized (having spatial order $n_c = n_d = 1$ in (9)), then it has the same value,

$$\hat{k}(\nu_j, z) = \frac{57.1599}{1 - z^{-1}} \cdot c(z) \tag{44}$$

for each spatial frequency $\nu_j \in \{\nu_1, \ldots, \nu_{54}\}$. The parameters of $c(z)$ are given by $\alpha_c = 0.8465$, $a_c = 0.7408$, and $d_c = 4$.

The integrator in the controller in (44) means that $|\hat{k}(\nu_j, e^{i\omega})| \to \infty$ as $\omega \to 0$, violating condition (42) for robustness. It could be argued that (42) is only a *sufficient* condition for robustness. However, in this case the necessary condition (29) also shows the stability margin becoming unacceptably small, $\hat{\beta}(\nu_j, \omega) \to |\hat{g}(\nu_j, 1)| \ll 0.08$ as $\omega \to 0$, for high spatial frequencies ν.

This situation is represented graphically in Figure 8 with a $\omega\nu$ contour plot in which the $|\hat{k}(\nu_j, e^{i\omega})| = 6.25$ contour for $\hat{k}(\nu_j, z)$ in (44) is plotted along with the set Ω_h in (43). Since this controller is independent of the spatial frequency ν, all contours of $|\hat{k}(\nu_j, z)|$ in (44) appear as vertical lines in the $\omega\nu$ plane. Figure 8 illustrates that the stability margin condition (42) is violated for high spatial frequencies ν and low dynamical frequencies ω. It is gratifying to find that this matches the qualitative description of the drifting, picketing instability illustrated in Figure 6.

In order to eliminate the closed-loop stability problems, the feedback controller was retuned according to the two-dimensional loop shaping procedure described in detail in Section V. Table II contains the resulting controller parameters. The spatial order of the controller was $n_c = 6$ and $n_d = 4$ corresponding to a localized feedback control law with $n_c, n_d \ll n = 54$. A comparison between Tables I and II shows that the controller parameters a_c and d_c do *not* match the model pole a and delay d as required by (31). This happened simply due the fact that one of the controller parameters was changed without our knowledge at the time of the test. This parameter defined the scanner traverse time (temporal sample time) used by the control system and subsequently altered the controller's interpretation of the discrete-time filter coefficients a_c and d_c in (7). The discrepancy was small enough as to go unnoticed in terms of the system performance at the time, and the analysis presented in this paper presents the controller parameters as they were implemented.

As in the previous section, the robust stability condition (42) is verified by plotting the $|\hat{k}(\nu_j, e^{i\omega})| = 6.25$ contour of the controller in (26), with parameters listed in Table II overlayed with the set Ω_h in (43). Figure 9 indicates that the robust stability condition (42) is now satisfied.

The controller parameters in Table II were installed in the working controller and observed over the course of 4 days, during which time the closed-loop system remained stable. Typical input and output profiles are displayed in Figure 10. Closed-loop performance is measured by the variation in the output profiles. The original controller settings listed in Table II resulted in an output variance of 0.248, as shown in Figure 6.

The more conservative controller designed by two-dimensional loop shaping resulted in an output variance of 0.254 as shown in Figure 10. However, the most remarkable difference evident from comparing Figures 6 and 10, is the appearance of the actuator profiles. The actuator profile variance was reduced by 32% with the new tuning numbers. This incurred only a 3% increase in the measured profile variance for the data in the figures shown. The reason that this can be achieved is due to the fact that the majority of actuation in Figure 6 is of such a high spatial frequency that it does not have a significant influence on the paper profiles due to the small process gain $|\hat{g}(\nu_j, z)|$ in (26) at high spatial frequencies as illustrated in Figures 4 and 5. However it should be noted that these figures display only a snapshot in time and the achievement of closed-loop stability led to a system that would provide reliable performance without daily operator intervention.

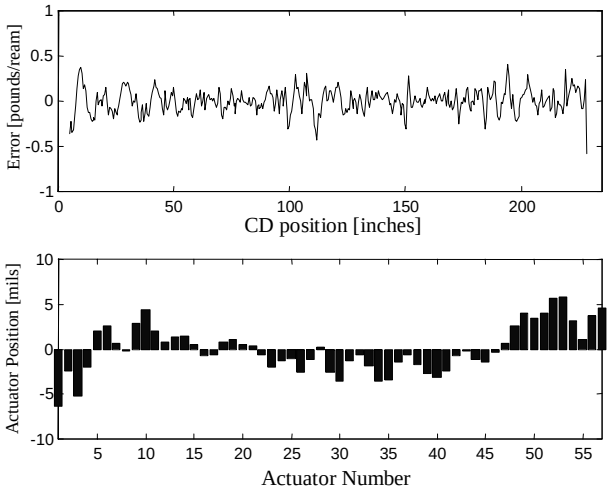

Fig. 10. Snapshot of typical closed-loop system performance with redesigned, localized controller $K(z)$ in (12), Table II corresponding to Figure 9. Note the reduction of high-spatial frequency actuation compared with Figure 6.

B. System 2: An Under-performing Consistency Profiling System

Consistency profiling is an alternative to the use of a slice lip for basis weight control [44]. These actuators change the basis weight profile by locally altering the concentration of pulp fibres in the headbox. This is accomplished by an array of dilution actuators distributed across the back of the headbox. The consistency of the pulp stock is changed by injecting it with a stream of low consistency water as it enters the headbox. An increase in the flow of a dilution actuator reduces the local concentration of pulp fibres and thus locally reduces the resulting basis weight.

The industrial implementation of consistency profiling falls into several different configurations. One configuration typically has $n = 150$ to 200 actuators with up to $n = 298$ actuators installed on 3.5cm centres. A second configuration typically has $n = 60$ to 80 actuators installed on 6.0cm to 7.0cm centres. Within the industry, there exist other consistency profiling systems with different configurations.

The response of the weight profile to a consistency profiling actuator is typically very well localized with none of the side lobes that may be observed in slice control, compare Figures 7 and 11. The typical effect of a consistency profiling actuator is confined to a 12.5cm strip centred on the actuator, and most of its influence being concentrated in the central 7.5cm.

As with the slice lip, the consistency profiling actuator dynamics are very fast compared with the scan time and the process dynamics are dominated by the sensor filtering and the transport delay.

The data in this section were taken from a Canadian paper machine, producing newsprint paper at a weight of 45 grams per square metre (45gsm) [33]. The paper profiles were measured with scanning gauge once every 25 seconds. These actuators are narrowly spaced at a separation of only 35mm and there were $n = 226$ on-sheet consistency profiling actuators - resulting in a very large scale control system.

Figure 11 illustrates the steady-state spatial response of the newsprint sheet to the consistency profiling actuators. The process model was identified from input-output data using the industrial software [19], [17]. The parameters of the model (3) representing the consistency profiling process are displayed in Table III.

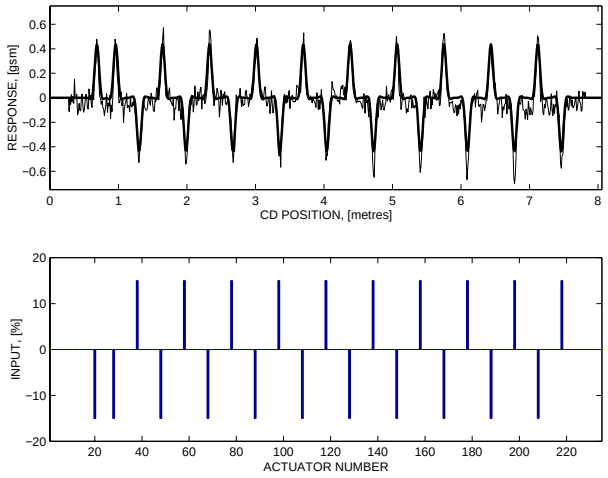

Fig. 11. The open-loop spatial response of the newsprint grade paper sheet to changes in the consistency profiling actuators.

Figure 12 illustrates the two-dimensional sensitivity function of the system running with the original tuning numbers. The plots indicate that the control system will eliminate disturbances with low spatial frequencies ν and low temporal frequencies ω, but will not remove high-frequency disturbances. In closed-loop the $\nu_{90} = 4.4$cycles/metre in (28), meaning that the system is expected to remove more than 90% of steady-state disturbances with a wavelength longer than about 23cm.

We logged 20 scans of closed-loop data from the system running with the original tuning numbers of the feedback controller listed in Table IV. The temporal average of these measurements is an approximation to the steady-state ($\omega = 0$) and the spatial frequency components of this system are plotted in Figure 13. As expected, this system is performing

Model parameter	Symbol	Identified value
number actuators	n	226
spatial order	n_b	5
spatial response	$\bar{b}$	[-4.8890, -2.8023, -0.3401, 0.0966, 0.0208] $\times 10^{-3}$
dead time	d	3
pole	a	0.8221

TABLE III

PROCESS MODEL PARAMETERS (3)–(5) FOR THE CONSISTENCY PROFILING SYSTEM.

Controller parameter	Symbol	Original tuning	Loop shaping tuning
decoupling spatial order	n_c	1	4
decoupling convolution	$\bar{c}$	[-106.4571]	[-67.5392, -31.7260, 15.1928, 15.3481]
smoothing spatial order	n_d	2	4
smoothing convolution	$\bar{d}$	[0.9595, 0.0202]	[0.9928, 0.0023, 0.0010, 0.0002]
internal model pole	a_c	0.7316	0.8221
internal model dead time	d_c	3	3
alpha	α_c	0.8365	0.8221

TABLE IV

CONTROLLER TUNING PARAMETERS (6)–(9) FOR THE CONSISTENCY PROFILING SYSTEM.

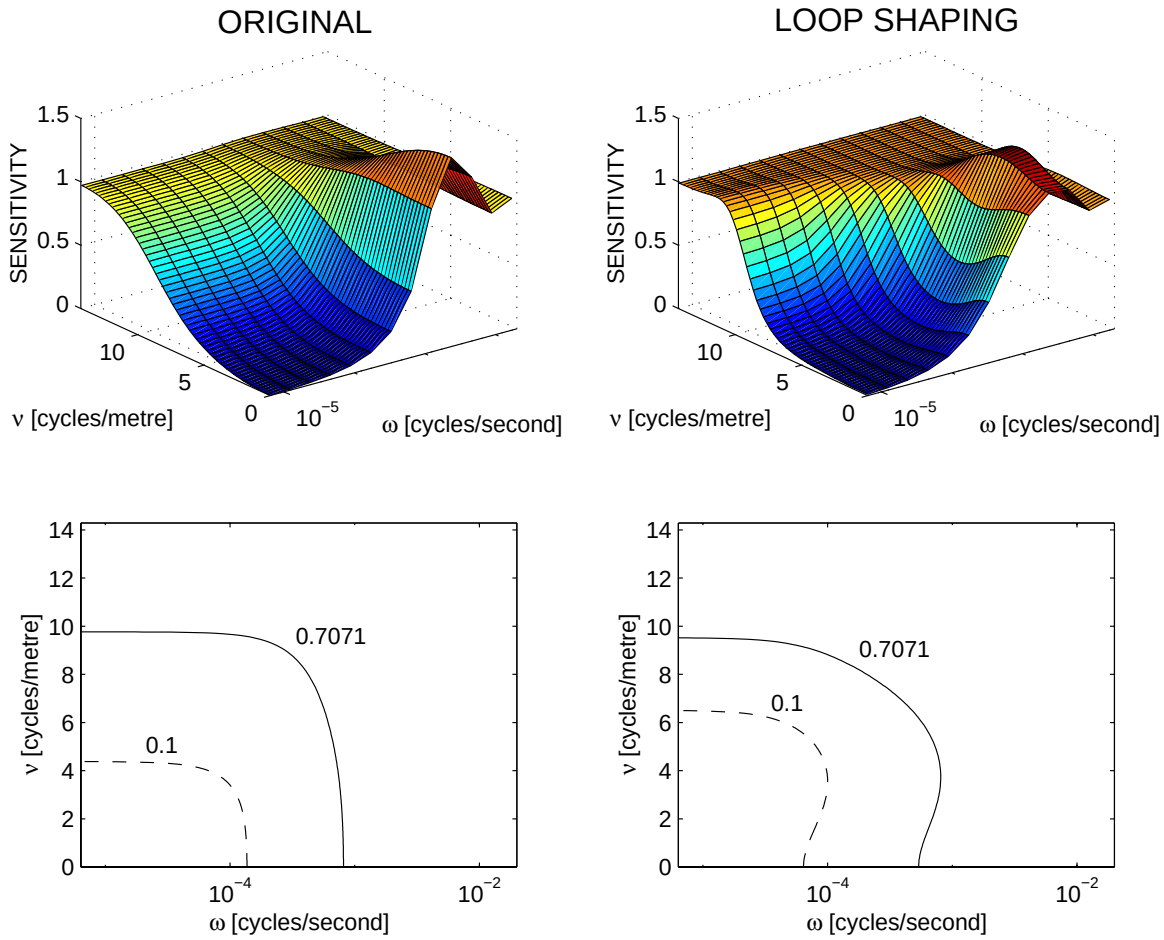

Fig. 12. Two-dimensional sensitivity functions plotted for the original tuning and the loop shaping tuning for the consistency profiling system. The contour plots are included to allow the comparison of the two-dimensional bandwidths for which $p = 10$ and $p = \sqrt{2}$ are satisfied in (28).

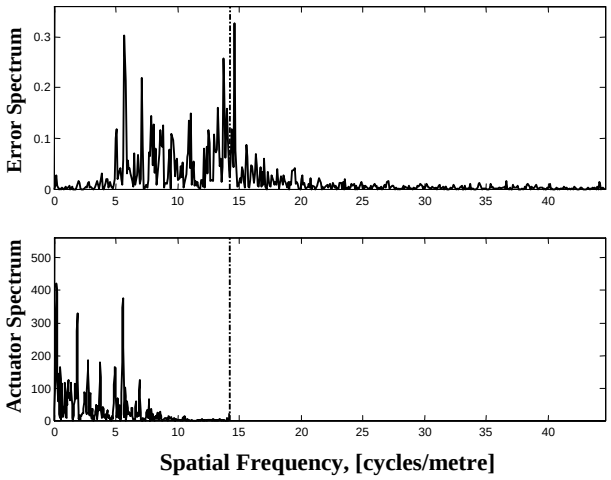

Fig. 13. The closed-loop steady state ($\omega = 0$) performance of the consistency profiling system under the original tuning. The vertical line indicates the spatial Nyquist frequency at two-times-actuator-spacing.

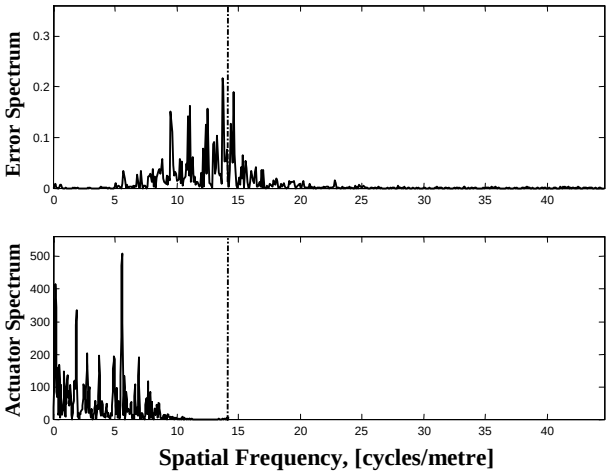

Fig. 14. The closed-loop steady state ($\omega = 0$) performance of the consistency profiling system under the loop shaping tuning. Note the reduced error and increased actuation in the $3\text{m}^{-1} < \nu < 8\text{m}^{-1}$ range compared with Figure 13.

better at low frequencies ν. There is very little error which persists at spatial frequencies lower than about 5 cycles/metre (wavelength of 20cm).

Next, using the two-dimensional loop shaping tuning tool outlined in Section V, we retune the cross-directional controller to achieve the sensitivity function illustrated in Figure 12. The contour plot indicates that the closed-loop spatial bandwidth has been improved to $\nu_{90} = 6.5$cycles/metre (a wavelength of about 15cm). This result predicts that the control system will be able to remove narrower disturbances from the paper sheet. Closed-loop data for the system running with the new tuning parameters was collected, and the steady-state spatial spectra for the error profile and the actuator profile are illustrated in Figure 14. With respect to the original tuning illustrated in Figure 13, the main difference may be seen at the 'mid-range' spatial frequencies roughly between 3m^{-1} and 8m^{-1} (a wavelength range of 13–33cm).

Improving the spatial bandwidth by retuning with the loop shaping tuning tool resulted in a reduction in steady-state variation of 26% in comparison with the original controller. This is considered a very significant performance improvement by a papermaker.

VII. Conclusions

This article has reported on the development and application of a novel controller design technique and its incorporation into an industrial software tool for cross-directional feedback controller tuning. Cross-directional (CD) control systems are spatially-distributed and are well known to be difficult to control. They are very large scale and typically severely ill-conditioned. Even the steady-state is not well-defined. In spite of these problems, the design of a CD control systems was made tractable and practical through the exploitation of the structure of the system. CD processes are linear, time-invariant, and almost spatially invariant systems. Appreciation of these features suggested the use of a two-dimensional frequency domain expansion, which led to the decoupling of the large-scale multivariable system into a family of SISO design problems, one for each spatial frequency.

The use of this two-dimensional frequency domain facilitated the development of a software tool for the tuning of an industrial CD feedback controller. The main algorithm used in this tool was outlined and its use on two different paper machines, experiencing very different problems was demonstrated.

The first machine was suffering from closed-loop instability problems. Our two-dimensional loop shaping tool was used to analyze the system and find its weakness - a vanishingly small stability margin. We were able to retune the cross-directional control system in order to achieve a robustly stable closed-loop system, as observed over 4 days of operation.

The second machine was apparently making good paper. However, the frequency domain analysis and subsequent retuning demonstrated that the system was not performing as well as it could. Prior to the use of the two-dimensional loop shaping controller tuning tool, the paper mill was not aware that their cross-directional control system was underperforming. Retuning this system was straightforward and improved the closed-loop spatial bandwidth and improved performance by 26%.

Acknowledgments

The authors would like to acknowledge the financial support of this work by Honeywell Industrial Control and the Natural Sciences and Engineering Research Council of Canada in the form of an Industrial Postgraduate Scholarship. The participation of Paul Baker and Cristian Gheorghe during the performance of the field trials described in this work is gratefully acknowledged.

REFERENCES

[1] A.P. Featherstone and R.D. Braatz, "Input design for large-scale sheet and film processes," *Ind. Eng. Chem. Res.*, vol. 37, pp. 449–454, 1998.

[2] D.L. Laughlin, M. Morari, and R.D. Braatz, "Robust performance of cross-directional control systems for web processes," *Automatica*, vol. 29, no. 6, pp. 1395–1410, 1993.

[3] S.R. Duncan, "The design of robust cross-directional control systems for paper making," in *Proc. of American Control Conf.*, Seattle, WA, USA, June 1995, pp. 1800–1805.

[4] S.R. Duncan, *The Cross-Directional Control of Web Forming Processes*, Ph.D. thesis, University of London, UK, 1989.

[5] A.P. Featherstone, J.G. VanAntwerp, and R.D. Braatz, *Identification and Control of Sheet and Film Processes*, Springer, 2000.

[6] K. Kristinsson and G.A. Dumont, "Cross-directional control on paper machines using gram polynomials," *Automatica*, vol. 32, no. 4, pp. 533–548, 1996.

[7] A. Rigopoulos, *Application of Principal Component Analysis in the Identification and Control of Sheet-Forming Processes*, Ph.D. thesis, Georgia Institute of Technology, USA, 1999.

[8] W.P. Heath, "Orthogonal functions for cross-directional control of web forming processes," *Automatica*, vol. 32, no. 2, pp. 183–198, 1996.

[9] S.-C. Chen and R.G. Wilhelm Jr., "Optimal control of cross-machine direction web profile with constraints on the control effort," in *Proc. of American Control Conf.*, Seattle, June 1986.

[10] W.P. Heath and P.E. Wellstead, "Self-tuning prediction and control for two-dimensional processes. part 1: Fixed parameter algorithms," *Int. J. Control*, vol. 62, no. 1, pp. 65–107, 1995.

[11] J. Fan, G.E. Stewart, and G.A. Dumont, "Model predictive cross-directional control using a reduced model," in *Control Systems 2002*, Stockholm, Sweden, June 2002, pp. 65–69.

[12] J.U. Backstrom, C. Gheorghe, G.E. Stewart, and R.N. Vyse, "Constrained model predictive control for cross directional multi-array processes," *Pulp and Paper Canada*, vol. 102, no. 5, pp. T128–T131, May 2001.

[13] J. Shakespeare, J. Pajunen, V. Nieminen, and T. Metsala, "Robust optimal control of profiles using multiple CD actuator systems," in *Control Systems 2000*, Victoria, BC, May 2000, pp. 306–310.

[14] G.E. Stewart, D.M. Gorinevsky, and G.A. Dumont, "Design of a practical robust controller for a sampled distributed parameter system," in *Proc. of IEEE Conference on Decision and Control*, Tampa, FL, USA, December 1998, pp. 3156–3161.

[15] G.E. Stewart, P. Baker, D.M. Gorinevsky, and G.A. Dumont, "An experimental demonstration of recent results for spatially distributed control systems," in *Proc. of American Control Conf.*, Arlington, VA, USA, June 2001, pp. 2216–2221.

[16] E.M. Heaven, I.M. Jonsson, T.M. Kean, M.A. Manness, and R.N. Vyse, "Recent advances in cross-machine profile control," *IEEE Control Systems Magazine*, pp. 36–46, October 1994.

[17] D.M. Gorinevsky, E.M. Heaven, C. Sung, and M. Kean, "Integrated tool for intelligent identification of CD process alignment shrinkage and dynamics," *Pulp and Paper Canada*, vol. 99, no. 2, pp. 40–44, 1998.

[18] D.M. Gorinevsky, R.N. Vyse, and E.M. Heaven, "Performance analysis of cross-directional process control using multivariable and spectral models," *IEEE Trans. on Control Systems Technology*, vol. 8, no. 4, pp. 589–600, July 2000.

[19] D.M. Gorinevsky and M. Heaven, "Performance-optimized applied identification of separable distributed-parameter processes," *IEEE Trans. Automat. Contr.*, vol. 46, no. 10, pp. 1584–1589, October 2001.

[20] D.M. Gorinevsky and C. Gheorghe, "Identification tool for cross-directional processes," *to appear in IEEE Trans. on Control Systems Technology*, 2003.

[21] P.J. Davis, *Circulant Matrices*, Wiley, New York, 1979.

[22] R.M. Gray, "Toeplitz and circulant matrices: A review," *http://ee-www.stanford.edu/˜gray/toeplitz.html*, 2001.

[23] K. Cutshall, "Cross-direction control," in *Paper Machine Operations, Pulp and Paper Manufacture, 3rd ed., vol. 7*, Atlanta and Montreal, Chap. XVIII 1991, pp. 472–506.

[24] D.W. Kawka, *A Calendering Model for Cross-Direction Control*, Ph.D. thesis, McGill University, Montreal, Canada, 1998.

[25] S.R. Duncan, P.E. Wellstead, and M.B. Zarrop, "Actuation, sensing, and two-dimensional control algorithms: Fundamental limitations on achievable bandwidths in MD/CD control," in *Tappi Proc. Process Control, Electrical and Information Conf.*, Vancouver, BC, Canada, March 1998, pp. 245–258.

[26] J.C. Skelton, P.E. Wellstead, and S.R. Duncan, "Distortion of web profiles by scanned measurements," in *Control Systems 2000*, Victoria, BC, May 2000, pp. 311–314.

[27] S.-C. Chen, "Full-width sheet property estimation from scanning measurements," in *Control Systems '92*, Whistler, BC, Canada, September 1992, pp. 123–130.

[28] S.R. Duncan and P. Wellstead, "Processing data from scanning gauges on industrial web processes," *submitted to Automatica*, August 2002.

[29] G.E. Stewart, J.U. Backstrom, P. Baker, C. Gheorghe, and R.N. Vyse, "Controllability in cross-directional processes: Practical rules for analysis and design," *Pulp and Paper Canada*, vol. 103, no. 8, pp. 32–38, August 2002.

[30] S. Skogestad and I. Postlethwaite, *Multivariable Feedback Control: Analysis and Design*, Wiley, New York, 1996.

[31] K. Zhou, J.C. Doyle, and K. Glover, *Robust and Optimal Control*, Prentice Hall, New Jersey, 1996.

[32] G.E. Stewart, D.M. Gorinevsky, and G.A. Dumont, "Two-dimensional loop shaping," *to appear in Automatica*, vol. 39, no. 5, May 2003.

[33] G.E. Stewart, *Two Dimensional Loop Shaping: Controller Design for Paper Machine Cross-Directional Processes*, Ph.D. thesis, Department of Electrical and Computer Engineering, University of British Columbia, Vancouver, Canada, 2000.

[34] B. Bamieh, F. Paganini, and M. Dahleh, "Distributed control of spatially invariant systems," *IEEE Trans. Automat. Contr.*, vol. 47, no. 7, pp. 1091–1107, July 2002.

[35] G. Ayres and F. Paganini, "Convex synthesis of localized controllers for spatially invariant systems," *Automatica*, vol. 38, no. 3, March 2002.

[36] R. D'Andrea and G.E. Dullerud, "Distributed control of spatially interconnected systems," *IEEE Trans. Automat. Contr.*, submitted.

[37] D.M. Gorinevsky and G. Stein, "Structured uncertainty analysis of robust stability for spatially distributed systems," in *Proc. of IEEE Conference on Decision and Control*, Sydney, Australia, December 2000.

[38] S.-C. Chen, P. Tran, and K. Kristinsson, "Closed-loop analysis and tuning of cross-direction (CD) control for sheet-forming processes," in *Proc. of IFAC Adchem*, Banff, Canada, June 1997, pp. 389–395.

[39] S.R. Duncan and G.F. Bryant, "The spatial bandwidth of cross-directional control systems for web processes," *Automatica*, vol. 33, no. 2, pp. 139–153, 1997.

[40] C. Langbort and R. D'Andrea, "Imposing boundary conditions for a class of spatially-interconnected systems," in *submitted to American Control Conf.*, Denver, Colorado, USA, June 2003.

[41] S. Mijanovic, G.E. Stewart, G.A. Dumont, and M.S. Davies, "Stability-preserving modification of paper machine cross-directional control near spatial domain boundaries," in *IEEE Conf. Decision and Control*, Las Vegas, Nevada, USA, December 2002.

[42] M. Hovd and S. Skogestad, "Control of symmetrically interconnected plants," *Automatica*, vol. 30, no. 6, pp. 957–973, 1994.

[43] G.A. Dumont, "Analysis of the design and sensitivity of the Dahlin regulator," Technical report, Pulp and Paper Research Institute of Canada, PPR 345 1981.

[44] R. Vyse, C. Hagart-Alexander, E.M. Heaven, J. Ghofraniha, and T. Steele, "New trends in CD weight control for multi-ply applications," in *TAPPI Update on Multiply Forming Forum*, Atlanta, Georgia, USA, February 1998.

PLACE PHOTO HERE

Gregory E. Stewart (S'97, M'00) received the B.Sc. degree in Physics in 1994 and the M.Sc. degree in Applied Mathematics in 1996 from Dalhousie University in Halifax, and the PhD degree from the Department of Electrical and Computer Engineering at the University of British Columbia in Vancouver in 2000.

He currently holds the position of Senior Control Engineer for Honeywell Industry Solutions and has held an Adjunct Professor appointment in the Department of Electrical and Computer Engineering at the University of British Columbia since 2000. His research interests are in the development and use of theory for practical implementation of advanced control strategies. His designs currently reside on more than 60 industrial installations.

Dr Stewart has received the IEEE "Control Systems Technology Award" (with Dimitry Gorinevsky), an NSERC "University-Industry Synergy Award for Innovation" (with Guy Dumont), and two Honeywell "Technical Achievement" awards (with Cristian Gheorghe).

PLACE PHOTO HERE

Dimitry M. Gorinevsky is a Senior Staff Scientist with Honeywell Labs (Aerospace Electronics Systems) and a Consulting Professor of Electrical Engineering with Information Systems Laboratory, Stanford University. He received Ph.D. from Moscow Lomonosov University and M.S. from the Moscow Institute of Physics and Technology. He was with the Russian Academy of Sciences in Moscow, an Alexander von Humboldt Fellow in Munich, and with the University of Toronto. Before joining Honeywell Labs he worked on paper machine control with Honeywell-Measurex and was an Adjunct Professor of Electrical and Computer Engineering at the University of British Columbia, Vancouver, Canada. His interests are in advanced information and control systems applications across many industries. He has authored a book, more than 110 reviewed technical papers and several patents. He is an Associate Editor of IEEE Transactions on Control Systems Technology. Together with Greg Stewart, he is a recipient of 2002 Control Systems Technology award of the IEEE Control Systems Society, in part, for industrial applications of the work described in this paper.

PLACE PHOTO HERE

Guy A. Dumont received his Diplôme d'Ingénieur from ENSAM, Paris, France in 1973 and his Ph.D., Electrical Engineering from McGill University, Montreal in 1977. In 1973-74, and then again from 1977 to 1979, he worked for Tioxide France. From 1979 to 1989, he was with Paprican, first in Montreal and then in Vancouver. In 1989, he joined the Department of Electrical and Computer Engineering at the University of British Columbia where he is a Professor and leads the Process Control Group. From 1989 to 1999, he held the Paprican/NSERC Chair in Process Control. In 2000-2002, he was also Associate Dean, Research for the Faculty of Applied Science. Guy Dumont was awarded a 1979 IEEE Transactions on Automatic Control Honourable Paper Award; a 1985 Paprican Presidential Citation; a 1990 UBC Killam research Prize; the 1995 CPPA Weldon Medal; the 1998 Universal Dynamics Prize for Leadership in Process Control Technology; the IEEE Control Systems Society 1998 Control Systems Technology Award; and NSERC Synergy Awards in both 1999 and 2002. He is a Fellow of the IEEE and the BC Advanced Systems Institute, and a member of ISA, PAPTAC and TAPPI. His current research interests are: adaptive control, distributed parameter system control, control loop performance monitoring, predictive control, with applications to the process industries, mainly pulp and paper, and more recently to biomedical engineering.